Ceramics-Silikáty 69 (3), 443-456 (2025)
www.ceramics-silikaty.cz doi: 10.13168/cs.2025.0027

PREDICTION OF THE COMPRESSIVE AND TENSILE STRENGTH OF HIGH-PERFORMANCE CONCRETE BASED ON A HYBRID MODEL OF MULTILAYER PERCEPTRON (MLP) AND LIGHTGBM

SHAOKA ZHAO*, YONG LUO**, JIANFENG LI***, ****, *****, #YIAN ZHOU******

*School of Big Data and Artificial Intelligence, Fujian Polytechnic Normal University Fuqing350300, China
**School of Civil Engineering, Engineering Campus, Universiti Sains Malaysia, Nibong Tebal, Penang14300, Malaysia
***Hainan Cloud Spacetime Information Technology Co., Ltd, Sanya572025, Hainan, China
****Xing Yun Chen (Hong Kong) Technology Limited, Hong Kong999077, China
*****College of Civil Engineering, Fuzhou University, Fuzhou Fujian, 350108, China
******Hunan Vocational College of Engineering, Changsha 410151, China

#E-mail: zhouyian1990@outlook.com

Submitted March 10, 2025, accepted April 24, 2024

Keywords: UHPC, MLP, LightGBM, Compressive Strength Prediction, Tensile Strength Prediction

With the increasing demand for the increasing performance of ultra-high-performance concrete (UHPC) in engineering construction, accurately predicting its compressive and tensile strength and optimising the material mix design has become a research focus. This paper proposes a hybrid model combining a multilayer perceptron (MLP) and LightGBM, which integrates the deep feature extraction capability of MLP and the efficient regression capability of LightGBM to achieve the high-precision prediction of UHPC compressive and tensile strength. Experimental data under different w/c (0.18, 0.19, 0.20, 0.22), curing temperatures (40 °C, 60 °C, 80 °C), and an ageing period of 56 days were collected for the model training and validation. The results show that the hybrid model outperforms the individual models, particularly exhibiting a high generalisation capability at low w/c, with R^2 reaching 0.98 in the validation and test sets and a mean absolute error (MAE) of only 1.02 MPa. Finally, the effects of different mix proportions and curing temperatures on the model's prediction results are discussed, providing valuable reference data for UHPC material design and engineering applications.

INTRODUCTION

With the rapid development of civil engineering and the growing demand for a sustainable infrastructure, high-performance construction materials have become a significant focus in modern engineering practices [1]. Ultra-high-performance concrete (UHPC) is widely used in critical structures, such as bridges, dams, tunnels, and high-rise buildings, due to its superior mechanical properties, including having high compressive and tensile strength, excellent fracture toughness, and durability. Compared to conventional concrete, UHPC has a denser matrix with a lower porosity, enhancing its resistance to chemical attack, chloride penetration, and cracking, making it ideal for projects requiring long service life and resilience under harsh conditions. Zhang et al. [2] conducted torsion tests on reinforced concrete (RC) beams strengthened with UHPC, demonstrating significant increases in the cracking and ultimate torsional capacity, with improvements reaching up to 488.5 % and 593.2 %, respectively. They highlighted the importance of surface roughening to improve the bonding between the UHPC and the RC substrate and found that three-sided wrapping was more effective than two-sided wrapping. Incorporating a steel reinforcement into the UHPC layer further enhanced the torsional strength and ductility, showing that performance gains can be achieved at a minimal additional cost. Xi et al. [3] investigated the use of red mud, an industrial by-product, as a mineral additive in UHPC to improve the sustainability. While red mud reduced the environmental impact of the UHPC production, it also decreased the workability and initial strength due to its lower cementitious properties. However, under high-temperature curing, UHPC with 40 % red mud achieved ultra-high compressive strength, indicating that the performance drawbacks can be mitigated through optimisation.

The exceptional performance of UHPC is mainly due to its optimised mix design, including cement, silica fume, ultrafine powders, superplasticisers, and steel fibres [4, 5]. Silica fume and ultrafine powders enhance the matrix packing, reducing the porosity and promoting the formation of C-S-H gels, which is critical for strength development. Steel fibres bridge cracks, increasing

the tensile strength and mitigating brittle failure. However, UHPC's complex composition and forming processes pose challenges for conventional strength prediction models, which struggle to capture non-linear relationships and account for variables such as the curing temperature, water-cement ratio, and fibre content [6, 7]. Therefore, developing more efficient predictive models that guide the mix design and improve the performance is a crucial research priority. By focusing on data-driven models, this study aims to address these limitations and provide reliable strength predictions to enhance UHPC's application in sustainable infrastructure development.

In recent years, machine learning (ML) techniques have gained attention in engineering materials research due to their capability to process complex non-linear data and deliver accurate predictions. Models such as artificial neural networks (ANNs), support vector machines (SVMs), and gradient boosting decision trees (GBDTs) have shown promise in predicting UHPC properties. For example, Uddin et al. [8] optimised UHPC formulations using a hybrid ANN model combined with the Modified Andreasen and Andersen (MAA) particle packing method, achieving higher accuracy than traditional methods. Wang et al. [9] used ANN, Gauss process regression (GPR), and particle swarm optimisation (PSO) to balance UHPC strength, flowability, and cost, while Chen et al. [10] demonstrated that a convolution neural network-gate recurrent unit (CNN-GRU) hybrid model produced the most accurate flowability predictions, highlighting the importance of mixture flow optimisation for structural durability.

Despite these advancements, the existing models face limitations. Multilayer Perceptrons (MLPs) are effective for capturing non-linear relationships, but are prone to overfitting, especially when applied to small datasets [11–13]. LightGBM, a gradient-boosting framework, offers fast training and better generalisation, but struggles to handle high-dimensional input data [14, 15]. To overcome these issues, this study presents a hybrid MLP-LightGBM model that combines MLP's feature extraction strength with LightGBM's efficient regression capability. The MLP module extracts latent non-linear features and transforms the input into high-dimensional representations, while LightGBM uses decision trees to fit the residuals and improve the prediction accuracy.

This research aims to:

Construct an MLP-LightGBM hybrid model to analyse data from various UHPC mix proportions, curing temperatures, and material compositions.

Evaluate the model's performance in predicting the UHPC compressive and tensile strengths and compare it to standalone MLP and LightGBM models.

Assess the model's effectiveness under different water-cement ratios and curing conditions to support the optimisation of UHPC formulations.

MODEL PRINCIPLE

This paper presents an advanced prediction method for determining the compressive and tensile strength of high-performance concrete (HPC) using a hybrid model that integrates the strengths of deep learning and the Light Gradient Boosting Machine (LightGBM). The primary goal of this approach is to harness the non-linear feature extraction capability of deep learning and the efficient regression capability of LightGBM to enhance the prediction accuracy and generalisation performance across various concrete formulations and curing conditions. By combining these two complementary techniques, the proposed hybrid model is designed to overcome the limitations associated with standalone predictive models, such as overfitting in deep neural networks and limited feature representation in traditional regression trees.

In this hybrid framework, a multilayer perceptron (MLP), which is a type of deep neural network, is employed to conduct deep representation learning of the input features derived from HPC mixtures. The input parameters include key material composition features, such as the water-cement ratio (w/c), cement content, silica fume, ultrafine powders, superplasticiser dosage, and steel fibre content, as well as external variables like the curing temperature and age. The MLP network comprises multiple hidden layers interconnected by non-linear activation functions, which enable the model to capture complex, non-linear interactions between the input features. Through iterative training, the network learns to optimise its internal weights, mapping the complex, high-dimensional input features into a low-dimensional latent space where the most representative key features are preserved. This feature mapping process is crucial for capturing underlying patterns that influence the mechanical properties of HPC.

The deep feature vectors generated by the MLP are then fed into the LightGBM model for regression prediction. LightGBM, a gradient boosting decision tree framework, excels at efficiently fitting complex residual errors by constructing an ensemble of weak learners (decision trees) that iteratively minimise the loss function. Unlike conventional boosting methods, LightGBM employs a leaf-wise growth strategy and a histogram-based binning approach, which significantly speeds up the training and reduces the memory consumption. Additionally, LightGBM's ability to handle categorical features, missing values, and large datasets makes it highly adaptable for predicting HPC properties in diverse experimental settings.

The output of the regression phase comprises predicted values for both compressive and tensile strength, offering comprehensive insights into the mechanical performance of the concrete under various conditions. This two-step process—feature extraction by the MLP and refined regression by LightGBM—ensures

that the hybrid model can accurately capture both the global trends and localised variations in the dataset, thereby improving robustness and generalisation.

MLP model structure

The Multilayer Perceptron (MLP) is a type of feedforward artificial neural network composed of an input layer, one or more hidden layers, and an output layer. Each layer consists of interconnected nodes (neurons), where each neuron applies a linear transformation followed by a non-linear activation function (commonly ReLU). The MLP is trained using a backpropagation algorithm to minimise the loss function, typically the mean squared error (MSE) for regression tasks. This allows the MLP to learn complex non-linear mappings between input features and the target output [16–18]. The MLP performs non-linear transformations on the input through a series of fully connected operations, and the output of each layer can be expressed as:

$$\mathbf{h}^{(l)} = f\left(\mathbf{W}^{(l)}\mathbf{h}^{(l-1)} + \mathbf{b}^{(l)}\right) \quad (1)$$

A commonly used activation function is ReLU (Rectified Linear Unit), which is expressed as:

$$f(x) = \max(0, x) \quad (2)$$

The loss function is expressed as:

$$\mathrm{L}_{MLP} = \frac{1}{n}\sum_{i=1}^{n}\left(y_i - \hat{y}_i\right)^2 \quad (3)$$

After the non-linear transformations of the MLP network, the original input features are mapped into a low-dimensional deep feature vector z, whose output form is:

$$\mathbf{z} = f_{MLP}(\mathbf{x}) \quad (4)$$

The feature vector z contains critical information related to the compressive and tensile strength of concrete, providing enhanced feature representation for subsequent regression tasks.

LightGBM model regression prediction

Its core principle is to build multiple weak learners (decision trees) and iteratively fit the residuals to minimise the loss function, thereby achieving regression prediction [19]. For a given sample set , the objective function of LightGBM can be expressed as:

$$\mathrm{L} = \sum_{i=1}^{n}\ell\left(y_i, \hat{y}_i\right) + \Omega(T) \quad (5)$$

where is the loss function, which is commonly chosen as the Mean Squared Error (MSE):

$$\ell\left(y_i, y_i\right) = \left(y_i - \hat{y}_i\right)^2 \quad (6)$$

Ω(T) represents the regularisation term, which is used to limit the model's complexity and prevent overfitting, where T denotes the structure of the decision tree. LightGBM performs node splitting by calculating the gradient information of each feature and selecting the feature that minimises the loss for partitioning. In addition, LightGBM uses a histogram-based acceleration algorithm to bucket continuous features, significantly speeding up the model training process. By continuously optimising the objective function, LightGBM ensures that the output predictions are as close as possible to the true values. In this method, the input to LightGBM is the deep feature vector z, and the output is the predicted compressive and tensile strength of the concrete.

$$\hat{y} = f_{LightGBM}(\mathbf{z}) \quad (7)$$

To further improve the performance of the model, an adaptive learning rate and regularisation strategy can be introduced. The loss function L can be further extended as follows:

$$\mathrm{L}_{\text{total}} = \alpha\mathrm{L}_{MLP} + \beta\mathrm{L}_{\text{LightGBM}} \quad (8)$$

EXPERIMENTAL

Materials

The selected cement is "Shaofeng 5'56 Ordinary Portland Cement," with a tested 28-day compressive strength of 52.5 MPa. The sand used is classified as a medium-coarse sand with a fineness modulus of 2.77. After washing and screening, it exhibits high purity and a well-graded particle size distribution, contributing to the improved workability and compressive strength of the concrete. The coarse aggregate consists of a mixture of limestone crushed stone and river pebbles, with a particle size range of 5 to 20 mm. The ratio of crushed stone to river pebbles is 7:3, and the overall crushing index is 7.41 %.

The superplasticiser used is a naphthalene-based high-performance superplasticiser, mainly composed of an ABC compound. The composite ultrafine fly ash powder is a secondary modified material, categorised into two types based on the dosage. The steel fibres used are end-hooked low-carbon cold-drawn fibres with a length of 30 mm, a diameter of 0.5 mm, and a tensile strength exceeding 1100 MPa.

Methods

The UHPC preparation process is illustrated in Figure 1. First, the cement, silica fume, ultrafine

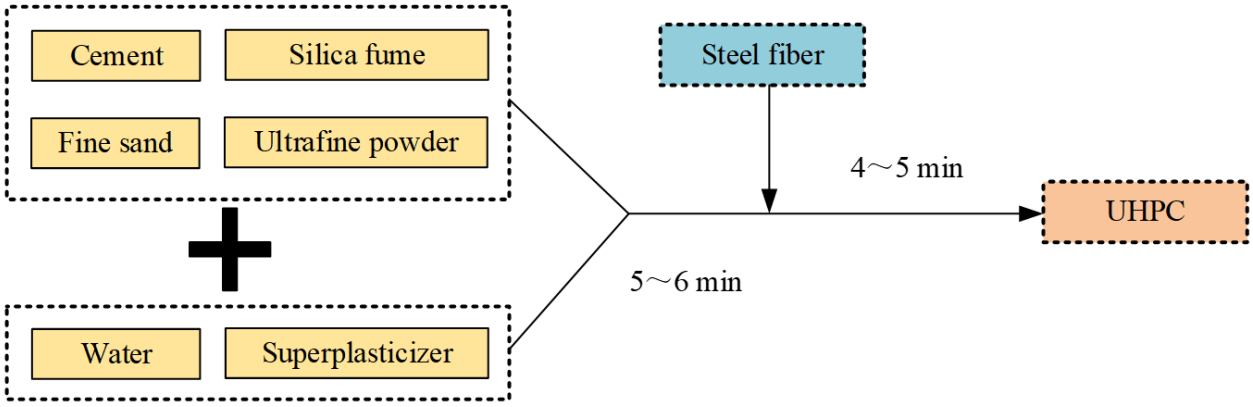

Figure 1. Preparation process of the high-strength UHPC.

Table 1. Mix proportions of the high-strength UHPC with different W/C ratios (kg·m³).

Material	W/C 0.18	W/C 0.19	W/C 0.20	W/C 0.22
Cement	950	900	880	850
Silica Fume	250	250	230	200
Ultrafine Powder	200	220	250	250
Fine Sand	950	950	950	950
Water	180	190	200	210
Superplasticiser	25	24	23	22
Steel Fibres	120	120	100	80

powder, fine sand, water, and the superplasticiser are added to a mixer as shown in Table 1. Water and the superplasticiser are added simultaneously and mixed for 5 to 6 minutes until a uniform slurry forms. After reaching a homogeneous consistency, steel fibres are gradually added, and mixing continues for another 4 to 5 minutes until the mixture flows smoothly along the mixer walls. Once the mixing is complete, the UHPC is poured into moulds for casting. To ensure reliability and reproducibility, each mix proportion was tested five times to minimise the variability and provide robust data for analysing the UHPC mechanical properties under different conditions as shown in Figure 2.

RESULTS AND ANALYSIS

Influence of the water-cement ratio on the mechanical properties of the UHPC under different curing temperatures

To investigate the effect of the W/C on the mechanical performance of the UHPC, compressive

a) Compressive Strength Test

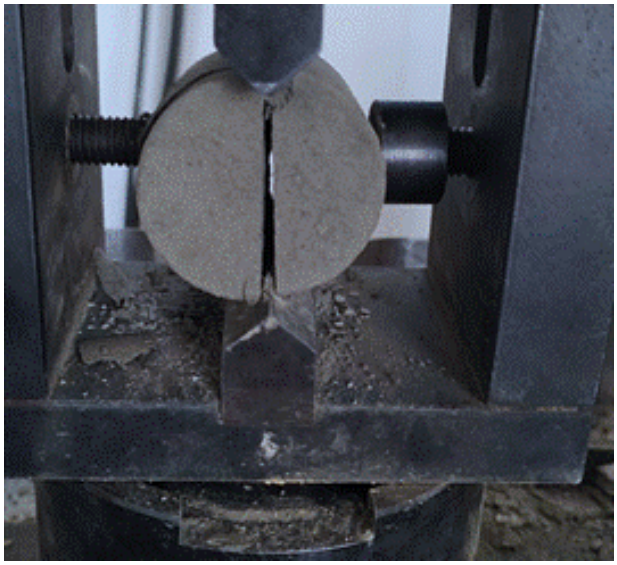

b) Tensile Strength Test

Figure 2. Test diagram of the specimens.

and tensile strength tests were performed on specimens with different W/C values (0.18, 0.19, 0.20, and 0.22) at curing temperatures of 40 °C, 60 °C, and 80 °C. The test results are shown in Figure 3.

The experimental data show that the compressive strength of the UHPC increases with the curing temperature at different W/C ratios. For a W/C of 0.18, the compressive strength at 40 °C is approximately 135 MPa. As the temperature rises to 80 °C, the strength fluctuates slightly, with a maximum value of 139 MPa, indicating high stability. This demonstrates that under a low W/C, the internal structure is dense with low porosity, and the temperature increase mainly accelerates the early hydration reactions, but has limited improvement on the long-term structural performance. For a W/C of 0.19, the compressive strength is about 147 MPa at 40 °C and increases to over 150 MPa at 80 °C, showing a significant enhancement. This is mainly due to the sufficient formation of the hydration products and a denser pore structure. The increase in temperature further promotes the formation of hydration products, significantly improving the compressive strength. For a W/C of 0.20, the compressive strength reaches about 156 MPa at 40 °C and increases to over 160 MPa at

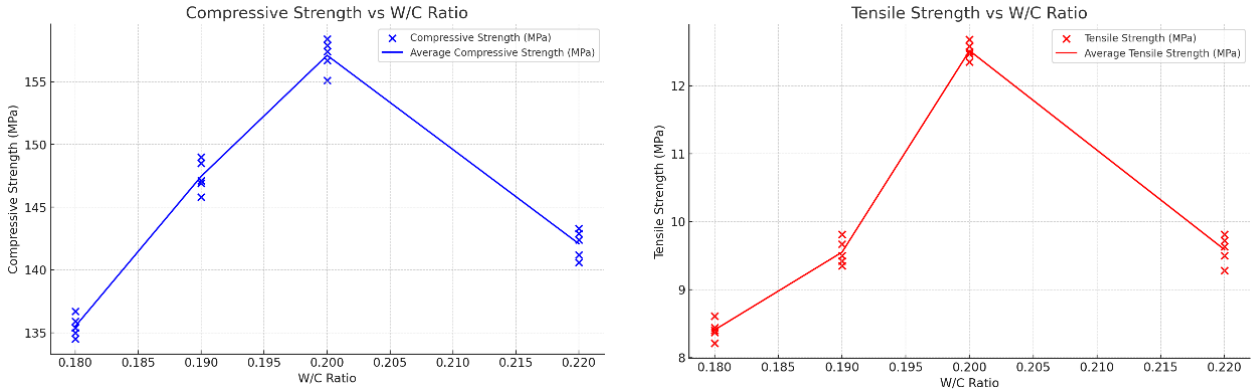

a) 40 °C

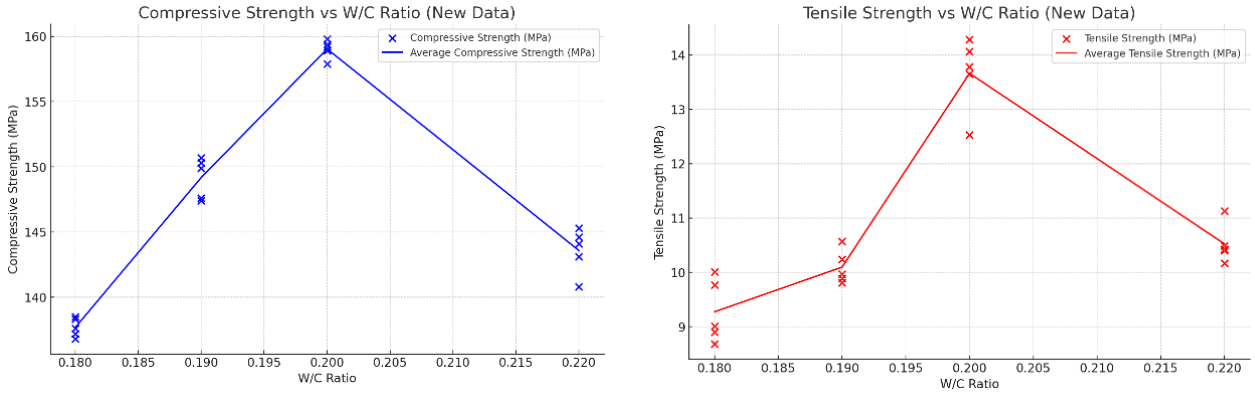

b) 60 °C

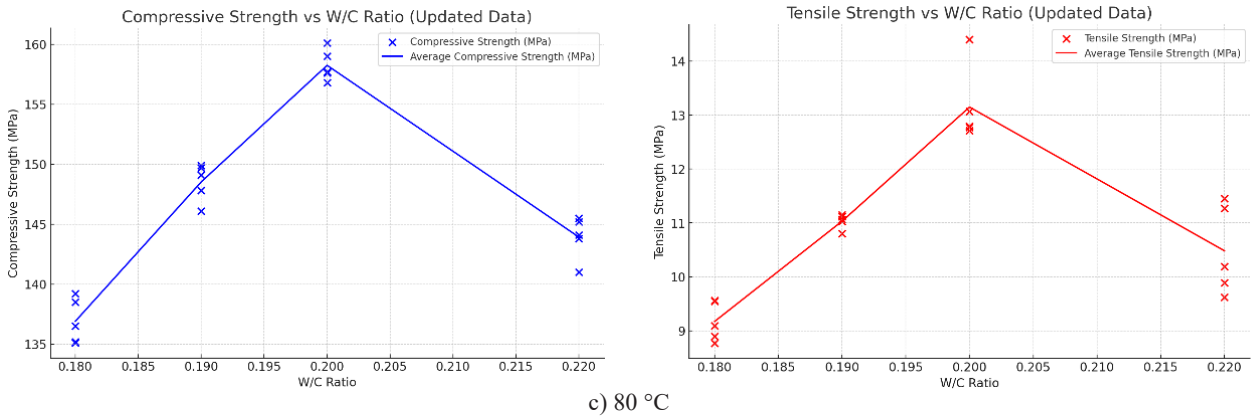

c) 80 °C

Figure 3. Scatter distribution of the mechanical properties under different W/C ratios.

80 °C, showing optimal compressive performance. This is because this W/C lies within the optimal range for C-S-H gel formation, resulting in low internal porosity and tighter interfacial bonding. For a W/C of 0.22, the compressive strength is about 142 MPa at 40 °C and about 145 MPa at 80 °C, but the increase is limited. This is mainly due to the high W/C, where the evaporation of excess water during steam curing forms more capillary pores, reducing the matrix's compactness and overall mechanical properties [20, 21].

The tensile strength trend is similar to that of the compressive strength, but with more significant variation. For a W/C of 0.18, the tensile strength at 40 °C is 8.4 MPa and increases to approximately 9.5 MPa at 80°C, showing good crack resistance. This is mainly due to a stronger fibre-bridging effect at low W/Cs, effectively inhibiting the crack propagation. For a W/C of 0.19 and 0.20, the tensile strength increases significantly at 60 °C and 80 °C, with a maximum value of 14.4 MPa, indicating that the optimal W/C enhances the bonding between the matrix and fibres. The dense C-S-H gel structure allows the fibres and the matrix to jointly bear the tensile stress, delaying the crack formation and propagation. For a W/C of 0.22, the maximum tensile strength at 80 °C is 11.45 MPa, which is inferior to the other ratios. This is mainly due to the excess residual water at high W/Cs, which weakens the bonding strength between the matrix and the fibres, reducing the fibre-bridging effect [22, 23].

Under high-temperature curing conditions, the improvement in the UHPC compressive and tensile strengths is mainly due to accelerated hydration reactions, which produce more C-S-H gel and increase the matrix's compactness. UHPC specimens with a low W/C have dense structures and fewer pores, limiting the effect of temperature on the strength improvement. In contrast, specimens with the optimal W/C exhibit significant fibre reinforcement effects and stronger interfacial bonding, enhancing both the tensile and compressive strength [24]. Specimens with a high W/C, however, suffer from the formation of capillary pores due to water evaporation, leading to reduced overall strength and crack resistance.

Effect of the curing temperature on the mechanical properties of the UHPC with different water-cement ratios

The curing temperature is a key factor affecting the mechanical performance development of UHPC. Under different temperature conditions, the compressive and tensile strengths of the UHPC specimens exhibit varying trends. This section focuses on analysing the mechanical properties of UHPC with a W/C of 0.18, 0.20, and 0.22 at curing temperatures of 40 °C, 60 °C, and 80 °C, as shown in Figure. 4.

For the UHPC with a W/C of 0.18, the compressive strength at 40 °C was approximately 135 MPa. As the curing temperature increased to 60 °C, the strength gradually increased to above 138 MPa, mainly due to the accelerated hydration reaction at higher temperatures, which generated more C-S-H gel and enhanced the matrix density. However, when the temperature increased to 80 °C, the strength fluctuated slightly or even decreased slightly, with some specimens exhibiting compressive strengths close to 135 MPa. This is attributed to overly intense early hydration reactions at high temperatures, causing internal-external temperature differences and resulting in micro-crack formation, thereby inhibiting further strength improvement. In contrast, the tensile strength showed a significant increase with the rising temperatures, reaching approximately 10 MPa at 60 °C and around 9.8 MPa in some specimens at 80 °C. This indicates that the fibre bridging effect was more pronounced at high temperatures, effectively enhancing the crack resistance.

For the UHPC specimens with a W/C of 0.20, the compressive strength at 40 °C was already over 156 MPa, demonstrating excellent mechanical properties. As the temperature increased to 60 °C and 80°C, the compressive strength further increased to about 159 MPa and 160 MPa, respectively. This suggests that under high-temperature conditions, the pozzolanic reactions of supplementary materials were further promoted, improving the internal matrix density and interfacial bonding strength. The tensile strength also increased significantly at 60 °C, with some specimens reaching over 14 MPa at 80 °C, indicating that the high-temperature environment further enhanced the bond between the matrix and fibres, forming a more stable bridging structure and thus improving the tensile strength.

For the UHPC with a W/C of 0.22, the compressive strength at 40 °C was around 142 MPa, lower than that of the specimens with ratios of 0.18 and 0.20. As the curing temperature increased to 60 °C, the strength rose to 145 MPa, but at 80 °C, some specimens exhibited a decline in strength. This is due to the evaporation of excess water in high W/C specimens at elevated temperatures, leading to more capillary pores and reducing matrix density, thereby limiting further strength enhancement. However, the tensile strength still improved significantly at 60 °C and 80 °C, reaching a maximum value of about 11.4 MPa, mainly due to the fibre reinforcement effect and the filling effect of C-S-H gel, which provided some crack resistance during high-temperature curing.

MLP-LightGBM-based mechanical properties model construction

Dataset and statistical description

To build a predictive model for the compressive and tensile strength of UHPC, this study collected experimental data under various conditions, including different W/Cs, curing temperatures, and curing ages (56 days), involving over 300 sets of experimental

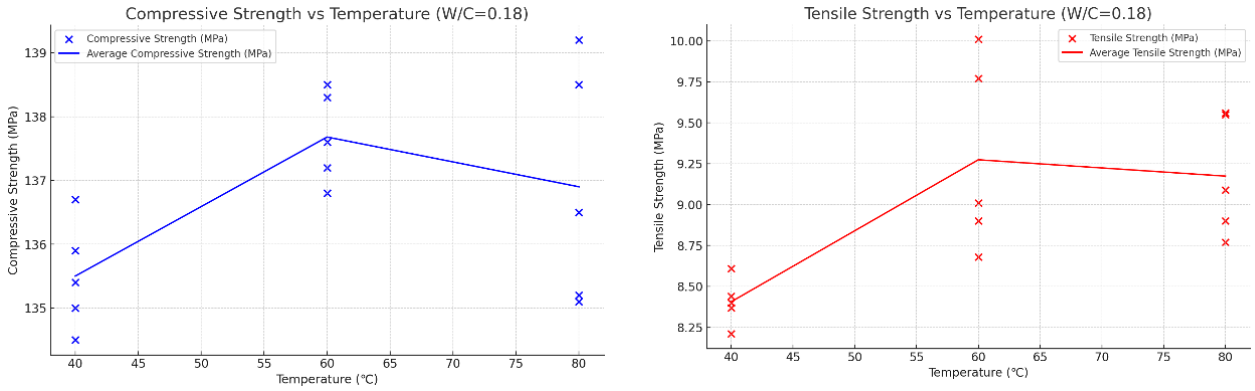

a) W/C = 0.18

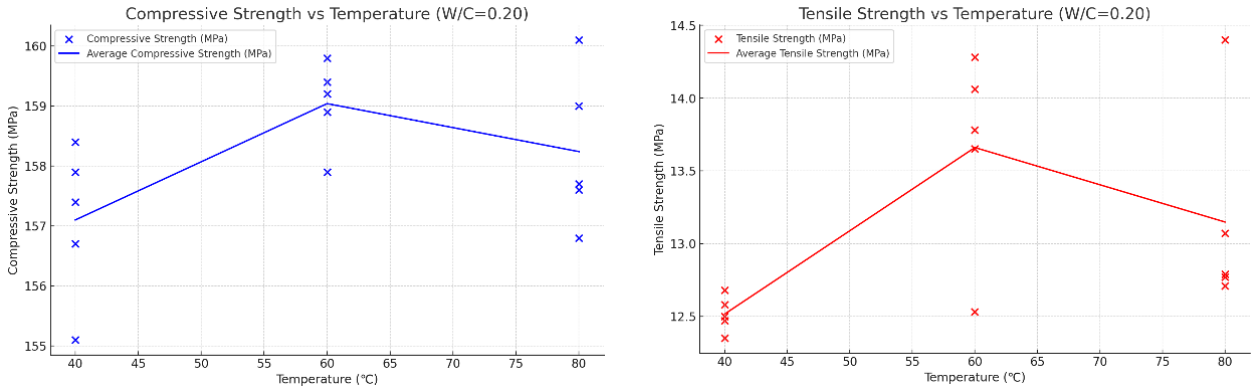

b) W/C = 0.20

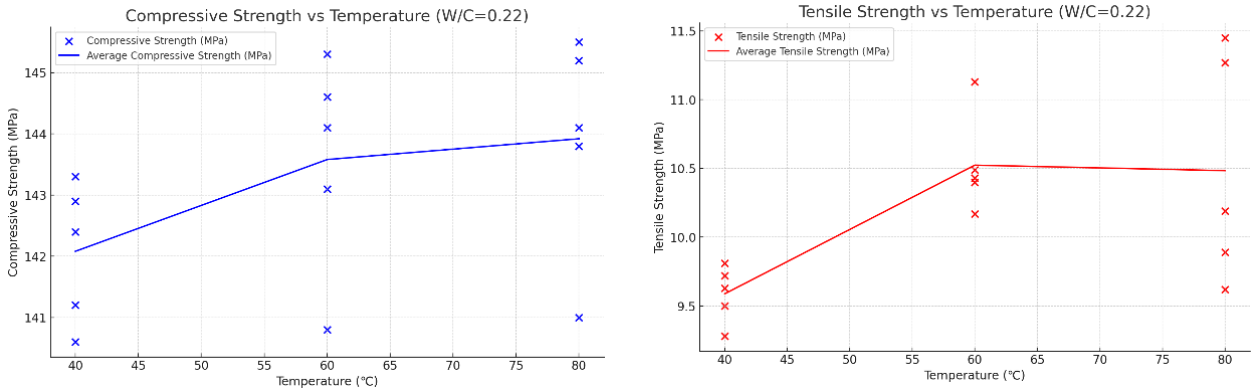

c) W/C = 0.22

Figure 4. Mechanical properties at different water to cement ratio W/C.

samples. Each data sample includes material parameters such as the cement, silica fume, ultrafine powder, fine sand, water, superplasticiser, and steel fibre content, as well as input features such as the W/C and curing temperature, and the output results for the compressive and tensile strengths. A correlation analysis of these indicators is shown in Figure 5.

The collected data underwent extensive pre-processing steps to ensure reliability and suitability for the machine learning analysis. This included conducting checks for missing values, identifying and removing outliers, and calculating key statistical descriptors for each feature. Table 2 presents a summary of the descriptive statistics, highlighting the central tendency, variability, and range of the dataset's variables.

The average water-cement ratio (W/C) across all the samples is 0.198, indicating that the dataset includes a balanced range of low, medium, and relatively high W/C values. This balance ensures that the model can capture the effects of both high and low W/C levels on the concrete's mechanical properties. The standard deviation of 0.015 for W/C indicates relatively small variations, ensuring the uniformity of the experimental conditions across the samples.

Table 2. Descriptive statistical results of the dataset.

Parameter	Mean	Standard Deviation	Min	Max
W/c	0.198	0.015	0.18	0.22
Cement ($kg \cdot m^{-3}$)	890	30	850	950
Silica Fume ($kg \cdot m^{-3}$)	240	12	200	250
Ultrafine Powder ($kg \cdot m^{-3}$)	230	20	200	250
Fine Sand ($kg \cdot m^{-3}$)	950	0	950	950
Water ($kg \cdot m^{-3}$)	195	10	180	210
Superplasticiser ($kg \cdot m^{-3}$)	23.5	1.5	22	25
Steel Fibre ($kg \cdot m^{-3}$)	100	15	80	120
Curing Temperature (°C)	60	16.33	40	80
Compressive Strength (MPa)	148.2	7.8	135	160.1
Tensile Strength (MPa)	10.8	1.9	8.2	14.4

The silica fume content varies between 200 and 250 $kg \cdot m^{-3}$, while the ultrafine powder content spans a similar range, reflecting diverse mix designs aimed at achieving optimal microstructural properties.

The fine sand content remains constant at 950 $kg \cdot m^{-3}$ across all the samples, indicating that this component was standardized to maintain consistency in the particle distribution and packing efficiency.

The superplasticiser dosage averages 23.5 $kg \cdot m^{-3}$, with a variation between 22 and 25 $kg \cdot m^{-3}$. The narrow range of superplasticiser content suggests careful optimisation to balance the flowability and strength while minimising the water demand.

The curing temperature spans from 40 °C to 80 °C, with an average of 60 °C and a standard deviation of 16.33 °C, encompassing standard, elevated, and high-temperature curing conditions. This variation allows the study to capture the effects of thermal curing on the hydration kinetics and microstructural development.

The statistical summary confirms that the dataset has a relatively uniform distribution of key input and output parameters, ensuring that no particular W/C ratio or curing temperature is overrepresented or underrepresented. This balance is crucial for training a predictive model that generalises well across different experimental conditions.

Furthermore, the correlation analysis illustrated in Figure 5 provides insights into the relationships between the input features and the mechanical performance. High correlations between the cement content and the compressive strength, as well as the steel fibre content and tensile strength, highlight the dominant contributions of these components to the overall mechanical behaviour. Conversely, the relatively weak correlation of the fine sand and superplasticiser content with the strength values suggests that these components primarily influence the workability and microstructure rather than directly enhancing the strength.

From the correlation matrix heatmap, it is evident that the cement content has a strong correlation with compressive strength, indicating that cement, as the primary cementitious material, significantly contributes to the overall strength development of concrete. In the mix design, a higher cement content enhances the compactness of the concrete matrix, promoting the generation of C-S-H gel and significantly improving the compressive performance. Similarly, the curing temperature also shows a strong positive correlation with the compressive strength, demonstrating that elevated temperatures can accelerate the hydration process, enabling concrete to achieve higher strength at an early age. However, in the case of high W/C, elevated temperatures may induce internal microcracks, thereby limiting further strength improvement.

The tensile strength is strongly correlated with the steel fibre content, reflecting the crucial role of steel fibres in improving the crack resistance and delaying the crack propagation in concrete. A proper amount of steel fibres can form a uniform bridging structure within the concrete, enhancing its stress dispersion capacity and improving the tensile performance. The W/C also correlates with the tensile strength, with a lower W/C contributing to higher matrix compactness and stronger interfacial bonding, thereby amplifying the fibre reinforcement effect.

In contrast, materials such as the fine aggregate, ultrafine powder, and silica fume exhibit relatively weak correlations with both the compressive and tensile strengths, indicating that these materials primarily improve the overall performance by filling the micro-pores and optimising the microstructures rather than directly enhancing the strength. Moreover, the correlation of the superplasticiser content with the strength is low, suggesting that its primary function is to improve the workability and fluidity rather than directly boosting the strength.

Model architecture and hyperparameter configuration

This study proposes a hybrid prediction method for mechanical performance based on a Multilayer

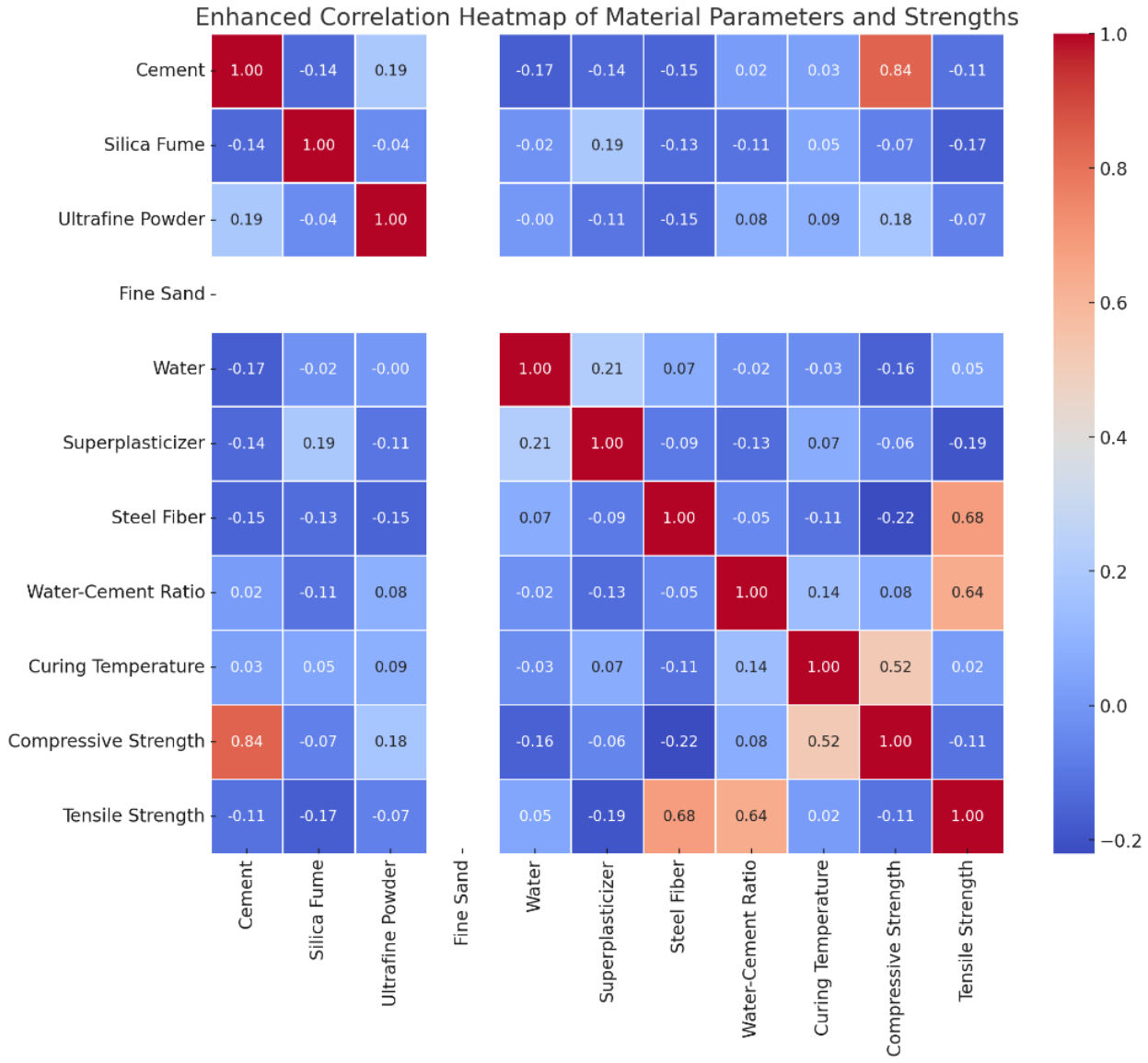

Figure 5. Correlation matrix heatmap.

Perceptron (MLP) and LightGBM, combining deep feature extraction with efficient regression to improve the prediction accuracy and generalisation capability. The input consists of the material parameters and mix design features of UHPC, while the output is a deep feature vector. This feature vector is fed into the LightGBM model for regression, generating predicted values for the compressive and tensile strengths.

LightGBM, serving as the regressor, performs ensemble learning through multiple decision trees. The key hyperparameters are set as follows:

Learning rate: 0.05
Maximum tree depth: 8
Number of decision trees: 200
Sub-sample ratio: 0.8
Regularisation parameters: $\lambda 1 = 0.1$, $\lambda 2 = 0.1$

After 30 epochs, the training and validation losses tend to converge, with minimal fluctuations in the validation loss, demonstrating that the model has good generalisation ability as shown in Figure 6. To prevent overfitting, an early stopping strategy is introduced during training, terminating the process if the validation loss shows no significant decline for 10 consecutive epochs. This ensures that the model maintains high accuracy while possessing strong generalisation performance.

The training loss and validation loss stabilise at low levels within 100 epochs, with no significant difference between them, indicating that the model demonstrates high robustness in handling complex feature extraction and efficient regression tasks. By employing appropriate hyperparameter settings and optimisation strategies, the hybrid model effectively leverages input features, thereby improving the prediction accuracy for the compressive and tensile strengths of the UHPC.

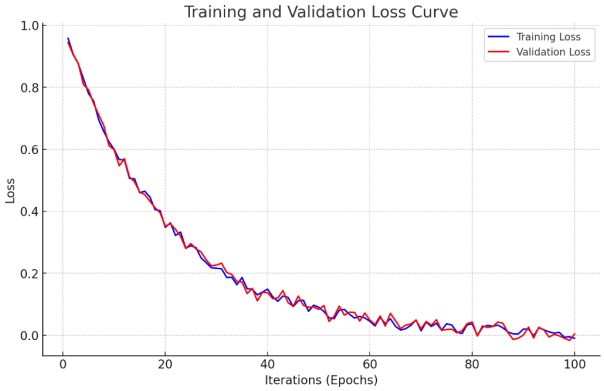

Figure 6. Model loss curve.

Model training and evaluation results

The model demonstrated excellent fitting performance on the training set, with the evaluation metrics on the validation and test sets presented in Table 3.

Table 3. Evaluation metrics for the validation and test sets.

Model Type	MAE	MSE	R^2
MLP-LightGBM	1.02	2.53	0.98
MLP	2.41	5.68	0.91
LightGBM	1.76	3.44	0.94

The results indicate that the MLP-LightGBM hybrid model outperformed the standalone MLP and LightGBM models in terms of MAE and MSE metrics. Notably, the R^2 value reached 0.98 on the test set, approaching the ideal value of 1.0, demonstrating that the hybrid model can effectively capture the complex non-linear relationships of the UHPC compressive and tensile strengths, exhibiting superior prediction accuracy and generalisation capability.

The MLP model, due to its deep learning structure, has strong feature extraction capabilities but is prone to overfitting, resulting in lower performance on the validation and test sets despite good training set performance. The LightGBM model, being a gradient-boosting decision tree-based regressor, effectively fits the data while avoiding overfitting, although it is less effective in handling high-dimensional and non-linear relationships.

By combining the strengths of MLP and LightGBM, the hybrid model extracts deep features through the MLP network and maps the input feature space into a low-dimensional latent space, eliminating redundant information while retaining key features. These deep features are then passed to LightGBM for regression, which refines the predictions by modelling the complex residuals using multiple decision trees. Additionally, early stopping and regularisation enhance the generalisation capability of the hybrid model, effectively preventing overfitting.

The hybrid model maintained minimal prediction errors for the compressive and tensile strengths across all the test samples, particularly for specimens with a W/C of 0.18 and 0.20, where errors were generally below 1.5 MPa, demonstrating excellent performance in low W/C conditions. For high W/C specimens (0.22), the model exhibited slightly larger errors due to the increased porosity and reduced structural density, yet the errors remained within an acceptable range.

Compressive strength prediction result analysis

For specimens with a W/C of 0.18 and 0.20, the prediction errors under different curing temperatures (40 °C, 60 °C, and 80 °C) generally remained below 1.5 MPa. At 60 °C, in particular, the predicted values aligned closely with the measured values, highlighting the model's capability to accurately interpret and learn the effects of elevated curing temperatures on the material properties. The MLP component effectively extracts hidden non-linear features from the input variables, transforming them into high-dimensional feature representations to enhance the expression of material characteristics. The LightGBM component, by employing an ensemble of decision trees to fit the residuals, refines the overall predictions and maintains the error levels within a minimal range (Figure 7).

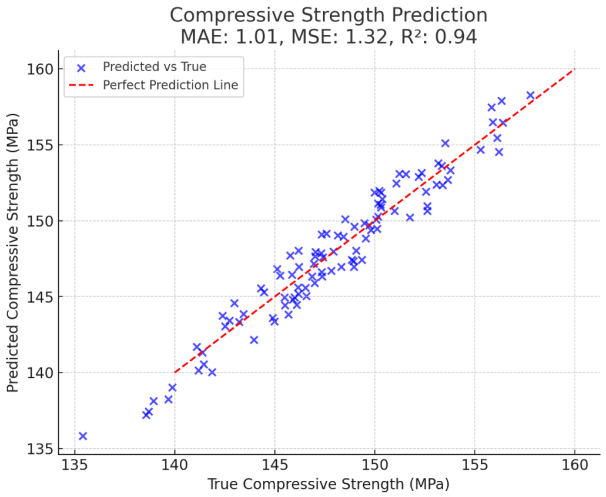

Figure 7. Scatter plot of the true vs. predicted compressive strength values.

For specimens with a water-cement ratio of 0.22, especially under the 80 °C curing condition, the predicted values were slightly lower than the measured results. This deviation can be primarily attributed to the evaporation of excess water in the high water-cement ratio mixtures under high-temperature curing, which leads to the formation of additional capillary pores. These pores reduce the structural density of the matrix and introduce greater variability in the measured compressive strength, highlighting the sensitivity of the model to microstructural changes in the concrete.

The MLP-LightGBM hybrid model also exhibited exceptional accuracy and robustness in predicting the tensile strength. As illustrated by the tensile strength scatter plot (Figure 8), the green data points were densely distributed near the ideal prediction line, demonstrating a strong agreement between the predicted and measured tensile strength values. In the test set evaluation, the model achieved a mean absolute error (MAE) of 0.28 MPa, a mean squared error (MSE) of 0.10 MPa², and a coefficient of determination (R^2) of 0.96, confirming the model's outstanding performance in the tensile strength prediction tasks.

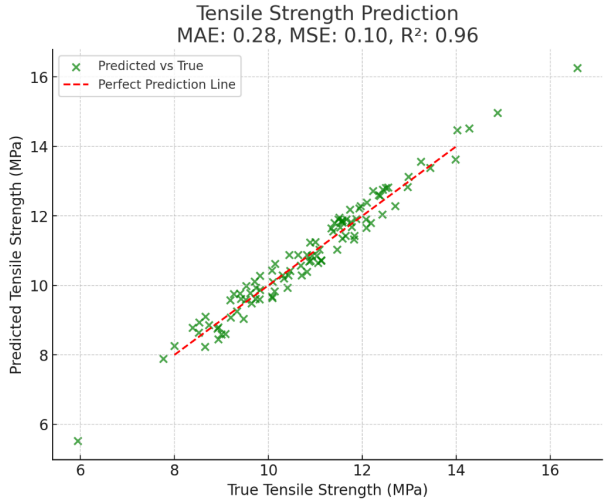

Figure 8. Scatter plot of the true vs. predicted tensile strength values.

For the specimens with W/C of 0.18 and 0.20, the tensile strength prediction error remained below 0.5 MPa. Under the elevated curing temperatures, the bridging effect of the steel fibres was significantly improved, effectively delaying the initiation and propagation of micro-cracks, thereby enhancing the tensile properties of the concrete. The hybrid model accurately captured this reinforcing effect, reflecting its ability to learn and represent the complex interactions within the composite structure.

In contrast, for the specimens with a water-cement ratio of 0.22, the prediction error showed a slight increase, but stayed within an acceptable range. This deviation can be attributed to the weaker interface transition zone (ITZ) commonly found in high water-cement ratio mixtures, which diminishes the bonding strength between the steel fibres and the matrix, causing minor fluctuations in the actual tensile strength measurements. The tensile strength prediction curves further indicate that tensile performance saw the most substantial improvement under 60 °C curing conditions. This finding suggests that an optimal curing temperature can significantly improve the bonding interface between the matrix and the steel fibres, thereby enhancing the stress transfer capability of the fibres and contributing to overall tensile strength improvements. This highlights the importance of selecting an appropriate curing temperature to optimise the microstructural integrity and mechanical performance of the UHPC.

DISCUSSION

In this study, the hybrid MLP-LightGBM model demonstrated exceptional performance in predicting the compressive and tensile strengths of ultra-high-performance concrete (UHPC). While the model effectively captured the non-linear relationships between the material composition, curing temperature, and mechanical properties, several aspects merit further discussion to provide insights into both the model's advantages and potential areas for improvement [25].

(1) Model robustness and accuracy: The evaluation metrics, including R^2, mean absolute error (MAE), and mean squared error (MSE), indicate that the hybrid MLP-LightGBM model performs significantly better than the standalone models. Particularly at a low W/C, the prediction errors for both compressive and tensile strengths were minimal. This demonstrates the hybrid model's ability to effectively learn and represent the interaction between UHPC's microstructural features and external factors, such as the curing conditions [26]. However, the slightly higher prediction errors observed at a higher W/C (e.g., W/C of 0.22) suggest that the model's performance could be influenced by the increased porosity of the matrix and the reduced bonding in the interface transition zone (ITZ). Therefore, future studies could focus on integrating additional features related to the pore structure and ITZ characteristics to enhance the prediction accuracy for high W/C mixes.

(2) Influence of the curing temperature on the model predictions: The results reveal that curing temperature plays a crucial role in the mechanical properties of UHPC. The hybrid model accurately captured the strength enhancements observed under 60 °C curing conditions, where the generation of calcium silicate hydrate (C-S-H) gel was optimal. Conversely, under the 80 °C conditions,

the formation of microcracks due to temperature-induced stresses limited further strength improvement. This highlights the importance of balancing hydration kinetics and thermal stress to optimise the material performance [27]. The model's accurate prediction of strength under varying temperatures also demonstrates its potential application in optimising curing regimes for specific construction requirements.

(3) Generalisation capability and data diversity: The model's generalisation capability was validated by its performance across different W/C ratios and curing conditions. Nevertheless, the accuracy of machine learning models depends heavily on the diversity and representativeness of the training dataset. Although the experimental dataset in this study covered a wide range of W/C ratios, curing temperatures, and mix compositions, the inclusion of additional variables, such as different fibre types, aggregate shapes, and supplementary cementitious materials, could further improve the robustness of the model in real-world applications [28].

(4) Implications for practical applications: The MLP-LightGBM hybrid model provides a reliable and efficient tool for predicting the UHPC performance, offering practical benefits for mix design optimisation and quality control. By accurately predicting the compressive and tensile strengths, engineers can make informed decisions about the material selection, curing procedures, and structural design. However, it is important to note that external factors, such as environmental humidity and specimen size, may influence mechanical properties in real construction projects. Incorporating these external variables into the model could improve its applicability to large-scale engineering projects [29].

(5) Future model improvements and interpretability: While the hybrid MLP-LightGBM model demonstrated high prediction accuracy, further research could focus on enhancing the model interpretability [30]. Techniques such as Shapley Additive Explanations (SHAPs) could be used to identify the contributions of individual input features to the predicted outcomes, thereby increasing the transparency and enabling more precise mix design adjustments. Additionally, ensemble learning methods incorporating recurrent neural networks (RNNs) could improve the model's ability to predict time-dependent properties, such as the strength development over different curing ages [31].

In summary, the hybrid MLP-LightGBM model provides a robust and accurate approach for predicting the mechanical properties of UHPC, particularly under variable curing conditions and mix proportions. Future research efforts should focus on expanding the dataset, integrating additional features, and enhancing model interpretability to further support the practical application of machine learning in UHPC performance prediction.

CONCLUSIONS

This study presents a hybrid prediction model combining Multilayer Perceptron (MLP) and LightGBM to accurately predict the compressive and tensile strengths of ultra-high-performance concrete (UHPC) under varying mix proportions and curing conditions. The model integrates the deep feature extraction capability of MLP and the efficient regression performance of LightGBM, achieving superior predictive accuracy compared to the individual models.

The model performed exceptionally well at a low W/C (0.18 and 0.20), where prediction errors for compressive and tensile strengths were generally below 1.5 MPa and 0.5 MPa, respectively, under curing temperatures of 40 °C, 60 °C, and 80 °C. The results indicate that at an optimal curing temperature of 60 °C, the UHPC specimens exhibited significant improvements in both the compressive and tensile strengths, reaching peak values of 159 MPa for compressive strength and 14 MPa for the tensile strength. This demonstrates that a moderate curing temperature can enhance the hydration process, increase matrix densification, and improve the bonding between the fibres and the matrix.

However, at a higher W/C of 0.22, the model exhibited slightly larger errors, particularly under the 80 °C curing conditions. This can be attributed to the evaporation of excess water, which led to the formation of additional capillary pores, reducing the matrix compactness and weakening the interface transition zone (ITZ). Despite this, the model still maintained acceptable prediction accuracy for these specimens, with a deviation remaining below 3 MPa.

The hybrid MLP-LightGBM model also demonstrated strong generalisation capability across different curing ages, as it was able to accurately predict strength variations at different time points. This highlights its potential to assist engineers in optimising UHPC mix designs and curing protocols. Additionally, the integration of early stopping strategies and regularisation improved the model's robustness and reduced the risk of overfitting.

REFERENCES

1. Zhang Y., Ren W., Chen Y., Mi Y., Lei J., Sun L. (2024): Predicting the compressive strength of high-performance concrete using an interpretable machine learning model. *Scientific Reports, 14*(1), 28346. doi: 10.1038/s41598-024-79502-z
2. Zhang Q., Jin Y., Wang G., Sun Q., Ghorbani, H. (2024): Improving stability and safety in concrete structures against high-energy projectiles: a machine learning perspective. *Frontiers in Materials, 11*, 1416918. doi: 10.3389/fmats.2024.1416918
3. Xi B., Li E., Fissha Y., Zhou J., Segarra P. (2024): LGBM-based modeling scenarios to compressive strength

of recycled aggregate concrete with SHAP analysis. *Mechanics of Advanced Materials and Structures, 31*(23), 5999-6014. doi: 10.1080/15376494.2023.2224782

4. Alghrairi N. S., Aziz F. N., Rashid S. A., Mohamed M. Z., Ibrahim A. M. (2024): Machine learning-based compressive strength estimation in nanomaterial-modified lightweight concrete. *Open Engineering, 14*(1), 20220604. doi: 10.1515/eng-2022-0604
5. Alhusban M., Alhusban M., Alkhawaldeh A. A. (2024): The efficiency of using machine learning techniques in fiber-reinforced-polymer applications in structural engineering. *Sustainability, 16*(1), 11. doi: 10.3390/su16010011
6. Aydın Y., Cakiroglu C., Bekdaş G., Geem Z. W. (2024): Explainable Ensemble Learning and Multilayer Perceptron modeling for compressive strength prediction of Ultra-high-performance concrete. *Biomimetics, 9*(9), 544. doi: 10.3390/biomimetics9090544
7. Cakiroglu C., Shahjalal M., Islam K., Mahmood S. F., Billah A. M., Nehdi M. L. (2023): Explainable ensemble learning data-driven modeling of mechanical properties of fiber-reinforced rubberized recycled aggregate concrete. *Journal of Building Engineering, 76*, 107279.doi: 10.1016/j.jobe.2023.107279
8. Uddin M. N., Ye J., Haque M. A., Yu K., Li L. (2024): A novel compressive strength estimation approach for 3D printed fiber-reinforced concrete: integrating machine learning and gene expression programming. Multiscale and Multidisciplinary Modeling, *Experiments and Design, 7*(5), 4889-4910. doi: 10.1007/s41939-024-00439-x
9. Wang Q., Qi J., Hosseini S., Rasekh H., Huang J. (2023): ICA-LightGBM algorithm for predicting compressive strength of geo-polymer concrete. *Buildings, 13*(9), 2278. doi: 10.3390/buildings13092278
10. Chen Y., Zeng J., Jia J., Jabli M., Abdullah N., et al. (2024): A fusion of neural, genetic and ensemble machine learning approaches for enhancing the engineering predictive capabilities of lightweight foamed reinforced concrete beam. *Powder Technology, 440*, 119680. doi: 10.1016/j.powtec.2024.119680
11. Dai J., Zhang Z., Yang X., Wang Q., He J. (2025): Machine learning prediction of concrete frost resistance and optimization design of mix proportions. *Journal of Intelligent & Fuzzy Systems, 48*(1-2), 47-72. doi: 10.3233/JIFS-236703
12. de-Prado-Gil J., Palencia C., Jagadesh P., Martínez-García R. (2022): A comparison of machine learning tools that model the splitting tensile strength of self-compacting recycled aggregate concrete. *Materials, 15*(12), 4164.doi: 10.3390/ma15124164
13. Golafshani E., Khodadadi N., Ngo T., Nanni A., Behnood A. (2024): Modelling the compressive strength of geopolymer recycled aggregate concrete using ensemble machine learning. *Advances in Engineering Software, 191*, 103611. doi: 10.1016/j.advengsoft.2024.103611
14. Tao H., Ali Z. H., Mukhtar F., Al Zand A. W., Marhoon H. A., Goliatt L., Yaseen Z. M. (2024): Coupled extreme gradient boosting algorithm with artificial intelligence models for predicting compressive strength of fiber reinforced polymer-confined concrete. *Engineering Applications of Artificial Intelligence, 134*, 108674. doi: 10.1016/j.engappai.2024.108674
15. Trinh S. H., Ly H. B. (2023): Enhancing Compressive strength prediction of Roller Compacted concrete using Machine learning techniques. *Measurement, 218,* 113196. doi: 10.1016/j.measurement.2023.113196
16. Schossler R. T., Ullah S., Alajlan Z., Yu X. (2025): Data-driven analysis in 3D concrete printing: predicting and optimizing construction mixtures. *AI in Civil Engineering, 4*(1), 1-25. doi: 10.1007/s43503-024-00044-4
17. Shafighfard T., Kazemi F., Asgarkhani N., Yoo D. Y. (2024): Machine-learning methods for estimating compressive strength of high-performance alkali-activated concrete. *Engineering Applications of Artificial Intelligence, 136*, 109053. doi: 10.1016/j.engappai.2024.109053
18. Su N., Guo S., Shi C., Zhu D. (2024): Predictions of mechanical properties of Fiber Reinforced Concrete using ensemble learning models. *Journal of Building Engineering, 98*, 110990.doi: 10.1016/j.jobe.2024.110990
19. Hosseini Sarcheshmeh A., Etemadfard H., Najmoddin A., Ghalehnovi M. (2024): Hyperparameters' role in machine learning algorithm for modeling of compressive strength of recycled aggregate concrete. *Innovative Infrastructure Solutions, 9*(6), 212. doi: 10.1007/s41062-024-01471-z
20. Qi R., Wu H., Qi Y., Tang H. (2024): Investigation of mechanical properties of high-performance concrete via multi-method of regression tree approach. *Materials Today Communications, 40*, 109922. doi: 10.1016/j.mtcomm.2024.109922
21. Qingfu L. (2025): Bayesian Optimization of Stacking Integrated Learning Model for Hpc Compressive Strength Prediction. article in press, available from: https://papers.ssrn.com/sol3/papers.cfm?abstract_id=5019913
22. Pakzad S. S., Ghalehnovi M., Ganjifar A. (2024): A comprehensive comparison of various machine learning algorithms used for predicting the splitting tensile strength of steel fiber-reinforced concrete. *Case Studies in Construction Materials, 20*, e03092. doi: 10.1016/j.cscm.2024.e03092
23. Poluektova V. A., Poluektov M. A. (2024): Artificial Intelligence in Materials Science and Modern Concrete Technologies: Analysis of Possibilities and Prospects. *Inorganic Materials: Applied Research, 15*(5), 1187-1198. doi: 10.1134/S2075113324700783
24. Nguyen H. A. T., Pham D. H., Ahn Y. (2024): Effect of Data Augmentation Using Deep Learning on Predictive Models for Geopolymer Compressive Strength. *Applied Sciences, 14*(9), 3601.doi: 10.3390/app14093601
25. Mustapha I. B., Abdulkareem M., Jassam T. M., AlAteah A. H., et al. (2024): Comparative analysis of gradient-boosting ensembles for estimation of compressive strength of quaternary blend concrete. *International Journal of Concrete Structures and Materials, 18*(1), 20.doi: 10.1186/s40069-023-00653-w
26. Mohammadi A., Barros J. A., Sena-Cruz J. (2025): An interpretable machine learning-based model for shear resistance prediction of CFRP-strengthened RC beams using experimental and synthetic dataset. *Compos. Struct, 351*, 118632. doi: 10.1016/j.compstruct.2024.118632
27. Marani A., Jamali A., Nehdi M. L. (2020): Predicting ultra-high-performance concrete compressive strength using tabular generative adversarial networks. *Materials, 13*(21), 4757.doi: 10.3390/ma13214757
28. Liu K., Zhang L., Wang W., Zhang G., Xu L., Fan D., Yu R. (2023): Development of compressive strength prediction platform for concrete materials based on machine learning techniques. *Journal of Building Engineering, 80*, 107977.

doi: 10.1016/j.jobe.2023.107977

29. Li Q., Song Z. (2023): Prediction of compressive strength of rice husk ash concrete based on stacking ensemble learning model. *Journal of Cleaner Production, 382*, 135279.doi: 10.1016/j.jclepro.2022.13527931.
30. Li Q., Ren G., Wang H., Xu Q., Zhao J., Wang H., Ding Y. (2023): Splitting tensile strength prediction of Metakaolin concrete using machine learning techniques. *Scientific Reports, 13*(1), 20102.doi: 10.1038/s41598-023-47196-4
31. Khandagale H. P., Salunkhe M. S., Kamble V. K., Manjarekar A. A., Halkarnikar P. P., Redekar S. S. (2024, August): Optimizing Concrete Compressive Strength Prediction: A Comparative Study of Machine Learning Algorithms. In *2024 International Conference on Electrical Electronics and Computing Technologies (ICEECT)* (Vol. 1, pp. 1-6). IEEE. doi: 10.1109/ICEECT61758.2024.10738970